BULLETIN OF THE POLISH ACADEMY OF SCIENCES
TECHNICAL SCIENCES, Vol. 73(1), 2025, Article number: e152605
DOI: 10.24425/bpasts.2024.152605

Machine learning-based filtering system for fNIRS signals analysis purpose

Mariusz PELC[1,2], **Dariusz MIKOLAJEWSKI**[3,4], **Adrian LUCKIEWICZ**[5], **Adam SUDOL**[6], **Patryk MENDON**[7], **Edward Jacek GORZELANCZYK**[8,9], and **Aleksandra KAWALA-STERNIUK**[10]*

[1] Institute of Computer Science, University of Opole, Opole, Poland
[2] School of Computing and Mathematical Sciences, University of Greenwich, London, UK
[3] Institute of Computer Science, Kazimierz Wielki University in Bydgoszcz, Bydgoszcz, Poland
[4] Neuropsychological Research Unit, 2nd Clinic of the Psychiatry and Psychiatric Rehabilitation, Medical University in Lublin, Lublin, Poland
[5] Faculty of Electrical Engineering, Institute of Theory of Electrical Engineering, Measurement and Information Systems, Warsaw University of Technology, Warszawa, Poland
[6] University of Applied Sciences in Nysa, Department of Technical Sciences, Nysa, Poland
[7] Faculty of Electrical Engineering, Automatic Control and Informatics, Opole University of Technology, Opole, Poland
[8] Kazimierz Wielki University in Bydgoszcz, Institute of Philosophy, Bydgoszcz, Poland
[9] The Society for the Substitution Treatment of Addiction "Medically Assisted Recovery", 85-791 Bydgoszcz, Poland
[10] Department of Artificial Intelligence, Faculty of Information and Communication Technology, Wroclaw University of Science and Technology, Wroclaw, Poland

Abstract. This paper presents a preliminary study delving into the application of machine learning-based methods for optimizing parameter selection in filtering techniques. The authors focus on exploring the efficacy of two prominent filtering methods: smoothing and cascade filters, known for their profound impact on enhancing the quality of brain signals. The study specifically examines signals acquired through functional near-infrared spectroscopy (fNIRS), a noninvasive neuroimaging modality offering valuable insights into brain activity. Through meticulous analysis, the research underscores the potential of machine learning approaches in discerning optimal parameters for filtering, thereby leading to a significant enhancement in the quality and reliability of fNIRS-derived signals. The results demonstrate the effectiveness of machine learning-based methods in optimizing parameter selection for filtering techniques, particularly in the context of fNIRS signals. By leveraging these approaches, the study achieves notable improvements in the quality and reliability of brain signal data. This work sheds light on promising avenues for refining neuroimaging methodologies and advancing the field of signal processing in neuroscience. The successful application of machine learning-based techniques highlights their potential for optimizing neuroimaging data processing, ultimately contributing to a deeper understanding of brain function.

Keywords: functional near-infrared spectroscopy; biomedical signal processing; machine learning; filtering, brain signals; smoothing filtering; cascade filtering.

1. INTRODUCTION

Brain signals are both electrical and chemical activity occurring within the brain, facilitating communication and coordination across various functions. Integral to brain function and information transmission within the nervous system, these signals are indispensable for proper neural processing [1–5].

Brain signals exhibit distinct characteristics owing to the diverse types of brain waves corresponding to different frequency ranges [1, 5]. Furthermore, the quality of signal acquisition equipment varies significantly; for instance, there exists a notable discrepancy between clinical electroencephalography (EEG) apparatus and EEG signal acquisition devices. Beyond equipment quality, two fundamentally different measuring techniques are employed. EEG focuses on capturing electrophysiological brain activation, detecting the electromagnetic field generated by firing neurons, whereas fNIRS utilizes hemodynamic response, tracking changes in blood oxygenation as brain regions become active. Given the differing sensitivities of EEG and fNIRS to various disturbances, which can evolve over time, it becomes apparent that devising alternatives to the conventional single-filter approach for signal filtering is imperative [6–11].

Grasping their fundamental mechanisms is crucial for progressing our comprehension of brain function, cognitive processes, and neurological disorders [1, 12, 13]. A range of techniques and methodologies are employed to explore and decipher brain signals, enriching our insight into how the brain processes information and underpins our thoughts, behaviors, and experiences [1, 4, 14, 15].

*e-mail: kawala84@gmail.com

Manuscript submitted 2024-05-14, revised 2024-10-20, initially accepted for publication 2024-10-22, published in January 2025.

In this paper authors decided to apply machine learning-based filtering system in order to analyze functional near-infrared spectroscopy signals.

1.1. Applied brain signals

Brain signals are classified based on their recording method and the invasiveness of their collection (see: Fig. 1) [1,2,15,16]. The authors focused on fNIRS signals only [1]. The fNIRSn signals yield multiple parameters, as noted in [10,17,18]. Among these parameters, HbR and HbT indicate changes in the concentration of deoxygenated hemoglobin and total hemoglobin, respectively. In fNIRS, these measurements assess alterations in tissue hemoglobin concentration [17,19].

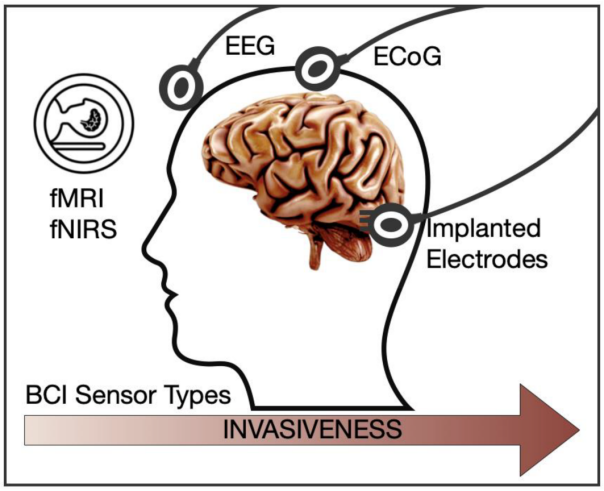

Fig. 1. Invasiveness of various brain signals [1, 15]

The HbR parameter indicates changes in deoxygenated hemoglobin concentration in tissue. When brain activity rises in a specific area, oxygen demand increases, causing a decrease in oxygenated hemoglobin (HbO) and an increase in deoxygenated hemoglobin (HbR) [17,20–22]. Thus, HbR serves as an indicator of cerebral blood flow changes linked to neural activity [21]. On the other hand, HbT reflects the total hemoglobin concentration, encompassing both oxygenated and deoxygenated forms [22–24]. It offers a measure of total blood volume in the tissue [23,24]. Changes in HbT may stem from diverse factors, including alterations in cerebral blood flow, blood volume, and oxygenation [22–26].

By concurrently measuring both HbR and HbO, changes in HbT can be computed using the following formula (1) [23,24]:

$$HbT = HbO + HbR. \tag{1}$$

The fNIRS gauges alterations in oxygenated and deoxygenated hemoglobin levels within the brain, offering an indirect indicator of brain activity. Utilizing near-infrared light, it evaluates fluctuations in blood oxygenation in the cerebral cortex. Importantly, fNIRS is a noninvasive technique [1,3,4,15,27,28].

Each form of brain signal offers distinct insights into various aspects of brain function, and they can frequently be applied together to provide more information [1,4,10].

2. MATERIALS AND METHODS

In order to acquire the brain signals, which are prone to various disturbances and artifacts [1, 29, 30], more legible appropriate filtering is necessary [30–32].

2.1. Measurement methods, configuration and study participants

The signals were obtained using the Cortivision fNIRS PHOTON+ cap [33] containing 12 channels, which consists of 12 light-sources and 10 detectors as illustrated with Fig. 2.

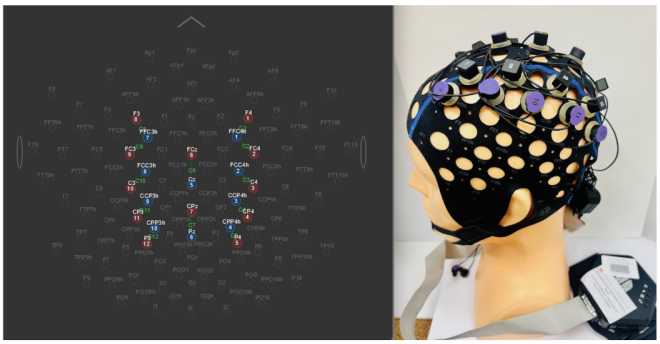

Fig. 2. Channel location (left) and the Cortivision cap (right)

The channels were located as follows: **Ch1:** $F4-FFC4h$, **Ch2:** $FC4-FFC4h$, **Ch3:** $C4-FCC4h$, **Ch4:** $CP4-CCP4h$, **Ch5:** $P4-CCP4h$, **Ch6:** FC_z-C_z, **Ch7:** CP_z-P_z, **Ch8:** $F3-FFC3h$, **Ch9:** $FC3-FFC3h$, **Ch10:** $C3-FFC3h$, **Ch11:** $C3-FCC3h$, **Ch12:** $CP3-CCP3h$, **Ch13:** $P3-CCP3h$.

This study analyzed data from a cohort of 30 healthy individuals. The research adhered to the principles outlined in the Declaration of Helsinki and obtained approval from the Bioethics Committee of the Nicolaus Copernicus University in Torun—Collegium Medicum in Bydgoszcz, Poland (protocol code no. KB 416/2008, dated September 17, 2008, valid until December 31, 2027). The database containing the signals is called "'Neuroimaging EEG and fNIRS Dataset (NERD)" and is openly available online [34].

The participant viewed a variety of images (see: Fig. 3), including positive, negative, and neutral as depicted with Fig. 4, while their brain activity was recorded.

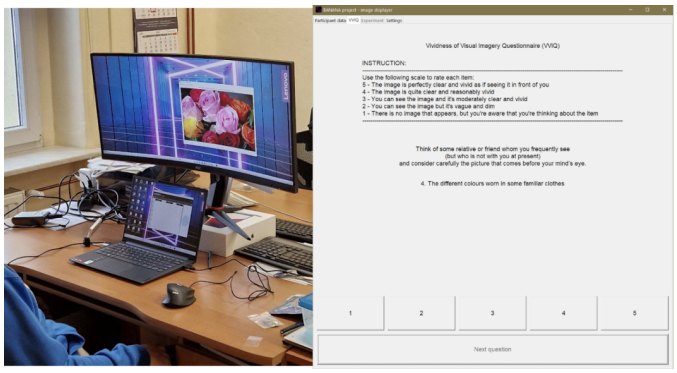

Fig. 3. Application for eye stimulation

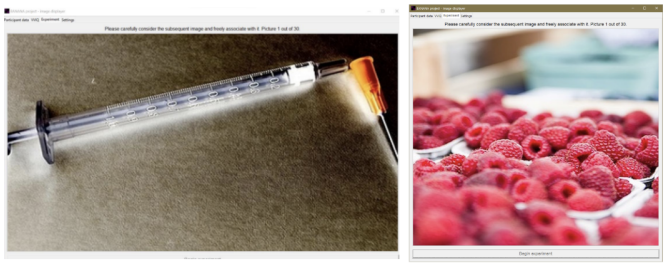

Fig. 4. Sample of displayed images: negative (left) and positive (right)

For the stimuli purposes the Open Affective Standardized Image Set (OASIS), an online stimulus set featuring 900 color images was applied [35]. The data can be found in [36] online repository.

2.2. Applied filtering

The theory of smoothing filters, particularly in the context of EEG data, has been recently reviewed in [15, 28, 29, 37].

When the disturbances are expected to have a specific distribution, then smoothing filtering may be the best approach [15, 28, 38, 39]. For this study purposes the authors applied moving average, Savitzky-Golay and Kalman filters, as illustrated with Fig. 5 [40, 41].

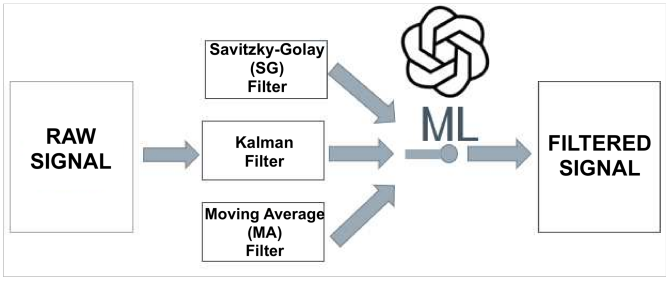

Fig. 5. ML–based filtering scheme

The selection of a smoothing filter relies on the specific application, noise characteristics, and the desired balance between noise reduction and signal detail preservation [42–46]. Each filter presents its unique strengths and weaknesses, and analyzing the signal frequency content or conducting experimentation can aid in identifying the most appropriate filter for a given scenario [29, 45, 47].

The simplest form of a smoothing filter is the moving average (MA) filter. This finite impulse response (FIR) filter, with length denoted as L, averages a certain number of samples of the signal to smooth it. Increasing the filter length reduces the true average of the signal and attenuates higher frequencies [42, 47]. In an MA filter of length L all coefficients are equal to $\frac{1}{L}$. Among the most popular smoothing filters are the Savitzky–Golay (SG) filters. These digital flat low-pass FIR filters are commonly applied to equidistant data points. SG filters rely on an nth degree polynomial fit within a symmetrical neighborhood around each data point k typically spanning from $k-m$ to $k+m$, while using $2m+1$ data points [29, 42, 48].

The Kalman filter [41] is frequently employed when disturbances adhere to a normal distribution [49]. It incorporates various construction parameters to consider signal and measurement variances. The 1D version of the Kalman filter is commonly utilized for signal smoothing tasks [49].

As far as filter parameters selection is concerned, the key design parameters of the Kalman filter were selected with respect to the signal parameters and specifically – its (estimated) variance being roughly around 0.1.

For the Savitzky-Golay filter the main design parameter is the filtration window width. Having a look at the signals one can see that the signal change which is of interest happens around $1800-1900s$. Taking into account the sampling frequency, we decided to choose window with 31 samples to not to overlook such change and on the other hand, to ignore at the same time changes resulting from filtration noise.

The chosen window width was allowing to calculate signal trend without being affected by the noise; and for the last of the filters – the moving average filter, the filtered value is being calculated based on the specific number of samples. For coherency reasons (to make this filter design related to the design of the Savitzky-Golay filter) the number of samples based on which a filtered value was calculated was chosen to be 31.

2.3. Test methodology

The ML training task was performed using a designated *CSV* file where the proper filter selection depending on the *signal change* value and *trend* value was specified. The training dataset is shown in Fig. 6.

```
   IW   filter_f.csv                                    Row 1    Col 22
Change,Trend,FilterNo
-.0062500000000000000,-1.000000,Filter3
-.0062250000000000000,-1.000000,Filter3
-.0062000000000000000,1.000000,Filter2
-.0061750000000000000,1.000000,Filter2
-.0061500000000000000,-1.000000,Filter3
-.0061250000000000000,-1.000000,Filter3
-.0061000000000000000,1.000000,Filter2
-.0060750000000000000,1.000000,Filter2
-.0060500000000000000,-1.000000,Filter3
-.0060250000000000000,-1.000000,Filter3
-.0060000000000000000,-1.000000,Filter3
-.0059750000000000000,0.000000,Filter2
-.0059500000000000000,0.000000,Filter2
-.0059250000000000000,1.000000,Filter2
-.0059000000000000000,-1.000000,Filter3
-.0058750000000000000,0.000000,Filter2
-.0058500000000000000,1.000000,Filter2
-.0058250000000000000,-1.000000,Filter3
-.0058000000000000000,-1.000000,Filter3
-.0057750000000000000,0.000000,Filter2
-.0057500000000000000,-1.000000,Filter3
```

Fig. 6. Dataset used for model training purposes

The filtered signal was provided in the *CSV* file (columns represent signal acquired from different sensors (see Fig. 7)).

Depending on the ML decision given as the result of the ML prediction, the ML filter output switched to the appropriate filter, respectively: *Filter 1* – Savitzky-Golay filter, *Filter 2* – Kalman filter and *Filter 3* – moving average filter. The code snippet showing ML-based filter selection is shown in Fig. 8.

For the test purposes a test application was developed in Python. Apart from three different filters implemented in this application (Savitzky-Golay [40], moving average [50] and Kalman filter [41]) the application also includes:

```
   IW   s6_10000.csv                                          Row 23   Col 1
C1_S1D1_1,C1_S1D1_2,C2_S2D1_1,C2_S2D1_2,C3_S3D2_1,C3_S3D2_2,C4_S4D3_1,C4_S4D3_2
0.5757326484,0.796967864,0.6211324334,0.8937638998,0.0254822168,0.0496691912,0.
0.5729321241,0.7980251908,0.6234766841,0.8981820941,0.0255459119,0.0498775616,0
0.5732153654,0.7918201685,0.6202555895,0.8914685845,0.0255333465,0.0497959219,0
0.5667867661,0.7870657444,0.6175216436,0.8861091137,0.0254780445,0.0497546382,0
0.5666353106,0.790958941,0.6172563434,0.8860833645,0.0255157501,0.0497101173,0.
0.5682021976,0.7883471251,0.619037807,0.8891213536,0.0255250484,0.0498167165,0.
0.5732910633,0.7974922061,0.6198040843,0.8911284208,0.0254955608,0.0498510599,0
0.5741935968,0.7949358225,0.6211360693,0.8941422701,0.0255490504,0.0499738045,0
0.5766967535,0.7996590137,0.6229346991,0.8979459405,0.0255515054,0.0501187518,0
0.5738447905,0.7990167141,0.6248544455,0.9016320109,0.0255675521,0.0502123125,0
0.5706019998,0.7932655811,0.6209987402,0.8933882713,0.0255441591,0.050160978,0.
0.5681332946,0.789177835,0.6189595461,0.8901811838,0.0255788341,0.0501069687,0.
0.5760752559,0.7962239385,0.6201534271,0.8930232525,0.025539875,0.0501170307,0.
0.5734068155,0.7910101414,0.6216395497,0.8954977393,0.0255579129,0.0502618663,0
0.5712386966,0.7965865135,0.622353971,0.897377193,0.0255854148,0.0502339043,0.0
0.5766180158,0.8003576994,0.623878181,0.90042907,0.0255785361,0.0503823273,0.02
0.5785425901,0.8062748313,0.6258376241,0.9046198726,0.025581928,0.0505361892,0.
0.5758274794,0.7967604399,0.6234727502,0.899282515,0.0255753957,0.0504481345,0.
0.5712468624,0.7932401896,0.6211976409,0.8950780034,0.0255851205,0.0503538512,0
0.5732858181,0.7986267209,0.621260643,0.8959093094,0.025570346,0.0504138656,0.0
0.5753409266,0.799898386,0.6227118373,0.8989084959,0.0255925432,0.0504811518,0.
0.5716315508,0.7987891436,0.62360394,0.900842905,0.0256272219,0.05055191,0.0215
```

Fig. 7. Example signal values

```
   I A  filter_f.py (python)  def gradually(csvname):          Row 82   Col 1
               result = mk.original_test(dataset_y[i-50:i, 0])
               if result.trend == 'increasing':
                    trend = "1"
               elif result.trend == 'decreasing':
                    trend = "-1"
               else:
                    trend = "0"
#               print("{},{}".format(change, result.trend))

               kwargs = {"Change":[change],"Trend":trend}
               filter = ml_predict(model, **kwargs)

               if filter == "Filter1":
                    yre.append(ykf[i])
               elif filter == "Filter2":
                    yre.append(ysg[i])
               else:
                    yre.append(yma[i])

    plt.plot(dataset_x, dataset_y[:,0], label='Noisy signal')
    plt.plot(dataset_x, ysg, 'r', label='Filtered signal SG, ws=31, order=1')
    plt.legend(loc="lower right")
    plt.title('Savitzky-Golay Filtering')
```

Fig. 8. Code snippet showing ML-based filter selection

- ML training module – this module allows training ML model based on the provided decision-making dataset (see Fig. 6);
- ML prediction module – this module based on the *Change* and *Trend* values specified value of which filter out of the 3 available and working in parallel filters should be used;
- Visualisation module – this module was responsible for graphical presentation of the filtering results.

As for the ML model trained for the ML-based filter selection we decided to use the *K-Nearest Neighbors* algorithm which provided accuracy at the level of **0.9841%**.

3. RESULTS

The results included in this section represent a pilot study and proof of concept implementation of ML-based filter selection. We have designed and implemented a system which will extract some desired features of the filtered signal and then these features will be used to train the ANN (Artificial Neural Network) model.

The key decision in successfully implementing this concept is determining the training data structure. This choice is crucial because it directly impacts the performance and accuracy of the Artificial Neural Networks (ANNs). In the simplest scenario, the input data for the ANN could be just the signal change value. Since noise typically has a limited amplitude compared to the signal, any significant change in the signal value would likely indicate a genuine step-change rather than noise. However, relying solely on signal change may not allow the ANN to distinguish between actual changes and slight variations caused by disturbances or noise.

To improve accuracy, additional features related to the signal (or environment, object characteristics, etc.) may be incorporated. For example, including the signal trend can provide better context for understanding specific signal changes. The more features considered, the more justified the use of ML/ANN becomes, as developing equivalent decision-making logic using traditional methods (such as *if/elif/else* statements) can be extremely challenging. Moreover, the flexibility and adaptability offered by ML/ANN training capabilities far surpass the potential of traditional reasoning systems, making them more suitable for complex filtering tasks.

In general, in order to use ML for filter selection it is necessary to extract certain signal features which could then be used on one hand, for neural model training purposes and on the other hand – these features being extracted on-line will allow choosing the best filter depending on the given signal parameters. Obviously, depending on which features will be selected and how they will be used to train the model one can expect more or less accurate signal filtering yet we decided to focus only on two of such features:

1) signal change – this property represents how the current signal sample differs from the previous one,
2) trend – this property allows representing the direction of the signal change.

These are only 2 parameters but the whole approach we present can be extended with any number of additional parameters and hence improve filter selection process.

Out of many existing trend analyzing algorithms including:

- Linear method,
- Mann-Kendall,
- Exponential growth method,
- Quadratic method,
- S-curve method,
- MAPE (mean absolute percentage error) method,
- MAD (mean absolute deviation) method,
- MSD (mean squared deviation) method.

We decided to use Mann-Kendall method [51] method. This was because this method can be used when the signal is measured with varying time periods or units and that this method can still be used in case certain values are missing in the set. This is very useful feature because in some cases it is difficult to measure the signal due to some physical property of the patient or the measured signal value is not very accurate due to e.g. disturbances. Another reason for choosing the Mann-Kendall method was that typically for trend analysis one of the key parameters is the number of samples used to determine a signal trend. Mann-Kendall method does not require this parameter instead it uses *significance level* parameter which is used to determine optimal number of samples to detect linear trend. In our case the significance level was at 0.05.

3.1. Test results

Using the test software we ran a number of filtering simulation tests in order to compare how the hybrid (ML-based) filter selection compares to the filtering results provided by each of the 3 co-operating filters independently.

Firstly, the *Savitzky-Golay* filter was tested. We chose *windows width* of value *31* and *order* of Filter *1*. Filtering results are shown in Fig. 9.

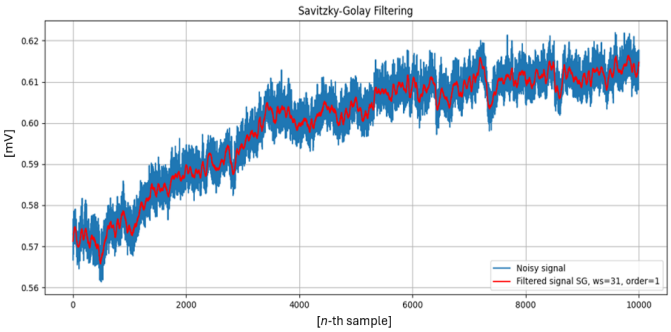

Fig. 9. Signal filtered using Savitzky-Golay filtering

Next, the *moving average* filter was tested. Its main design parameter is *window width* which we set at the value of *30*. The resulting filtering results are presented in Fig. 10.

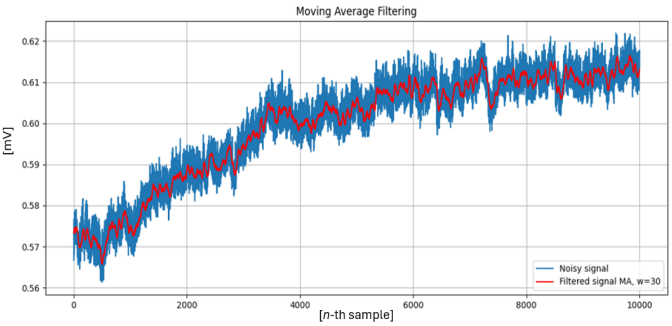

Fig. 10. Signal filtered using moving average filter

For the Savitzky-Golay filter and for the moving average filter the window width was chosen based on the estimated duration (the number of samples) of the signal value change caused by disturbance(s).

Thirdly, we decided to test the *Kalman* filter. In Fig. 11 we present filtering results with the design parameter *process noise variance* of value *0.0001*.

Last of the tested filters was the *ML-based filter*, This filter is in a sense virtual because here the filtered value is originating from one of the 3 main co-operating filters whilst the ML role was only to point at the value to be used in the specific situation. Filtering results are shown in Fig. 12.

Although at the first glance Figs. 9–12 look very similar, there are some differences between them. Each of the filters was tuned up so that they would perform the filtration task in the optimal way. However, the ML-based filter returns signal

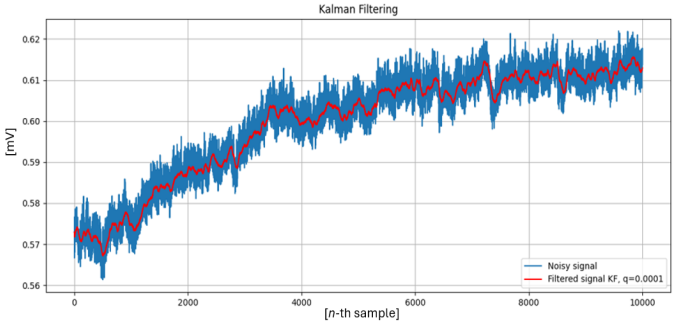

Fig. 11. Signal filtered using Kalman filter

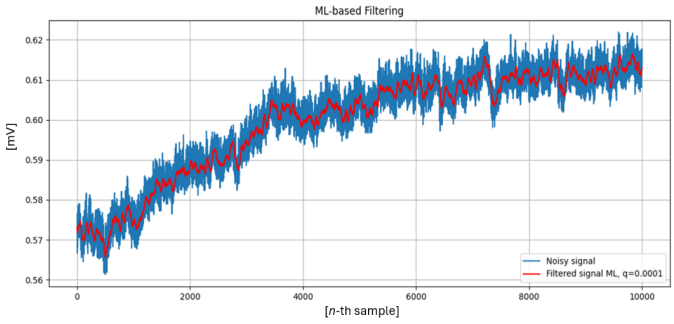

Fig. 12. Signal filtered using ML-based filter

which, depending on the circumstances, is a collation of signals generated by each of the filters. As a whole, it is not identical to any of the signals originating from filters working independently but zooming the picture would reveal that the ML-based signal works best.

In order to compare how the different filters perform in a more pronounced way, for each of the filters the overall variance of the filtered signal was calculated. Four different ML models were trained for the comparison *LogisticRegressioin*, *SVC*, *KNN* and *Gaussian*. These all models come from the Python's *module* and are all simple one-layer models (absolutely sufficient for this task) with the number of input neurons corresponding to the specified number of input columns from the dataset. Contrary to some other Python's modules (e.g. *Keras* model, these models do not provide functions allowing to check their exact structure (e.g. *Keras* model provides *layers* property containing information abut the number of model layers) as the structure is easy to determine just by considering the parameters of the training dataset.

As it was shown in Fig. 13, depending on which ANN model was trained for filters selection in the ML/hybrid mode, in each case the variance of the signal filtered by the ML-powered filter was the lowest. Compared to the next best filter (moving average), the ML-based filter performed around 8% better, while compared to the worst of the three base filters (Kalman filter), the ML-based filter preformed around 26% better. Overall, the average increase in performance was around 17% which proves that using AI for best filter selection allows a significant increase of filtering accuracy.

```
(myML) mariusz@ThinkPad:~/myML$ ./PES_18.py ./s12_500.csv
LRE Reading model from disk...

The variance of SG signal : 1.6474143609402187e-06
The variance of MA signal : 1.5412155340799853e-06
The variance of KF signal : 1.9046377826296131e-06
The variance of ML signal : 1.4145270184375988e-06

(myML) mariusz@ThinkPad:~/myML$ ./PES_18.py ./s12_500.csv
GAU Reading model from disk...

The variance of SG signal : 1.6474143609402187e-06
The variance of MA signal : 1.5412155340799853e-06
The variance of KF signal : 1.9046377826296131e-06
The variance of ML signal : 1.4212253159885521e-06

(myML) mariusz@ThinkPad:~/myML$ ./PES_18.py ./s12_500.csv
SVC Reading model from disk...

The variance of SG signal : 1.6474143609402187e-06
The variance of MA signal : 1.5412155340799853e-06
The variance of KF signal : 1.9046377826296131e-06
The variance of ML signal : 1.4145270184375988e-06
(myML) mariusz@ThinkPad:~/myML$ ./PES_18.py ./s12_500.csv
KNN Reading model from disk...

The variance of SG signal : 1.6474143609402187e-06
The variance of MA signal : 1.5412155340799853e-06
The variance of KF signal : 1.9046377826296131e-06
The variance of ML signal : 1.4266427025928533e-06
```

Fig. 13. Comparison of filtered signals variance

4. CONCLUSIONS AND DISCUSSION

Analyzing HbR and HbT signals in fNIRS can offer valuable insights into brain activation patterns, functional connectivity, and hemodynamic responses linked to cognitive processes. This makes fNIRS a valuable tool in cognitive neuroscience and neuroimaging research [23, 25, 26, 52].

In this paper, the authors decided to apply a machine learning-based filtering system to analyze functional near-infrared spectroscopy signals.

Although Figures above (in the Results section) may appear similar at first glance, there are notable differences between them. Each filter was optimally tuned to perform the filtration task effectively. The ML-based filter, however, produces a signal that integrates aspects of the signals generated by each individual filter. This integration means the ML-based signal is not identical to any single filter output. However, a closer examination reveals that the ML-based filter outperforms the others by providing a more accurate and reliable signal. This superiority is evident when zooming in on the signal, where the ML-based approach demonstrates its ability to handle variations and noise more effectively.

To sum it all up – analysis of the fNIRS and other brain signals is a very challenging task due to the complexity and variability of the signals involved. The brain's activity is influenced by numerous factors, including physiological and environmental conditions, making it difficult to extract meaningful information. Noise and artifacts further complicate the analysis, requiring sophisticated filtering and signal processing techniques to obtain accurate results. The use of advanced methods, such as machine learning-based filters, helps address these challenges by providing more robust and adaptive solutions for signal analysis.

REFERENCES

[1] A. Kawala-Sterniuk *et al.*, "Summary of over fifty years with brain-computer interfaces—a review," *Brain Sci.*, vol. 11, no. 1, p. 43, 2021.

[2] J. Uchitel, E.E. Vidal-Rosas, R.J. Cooper, and H. Zhao, "Wearable, integrated EEG–fNIRS technologies: A review," *Sensors*, vol. 21, no. 18, p. 6106, 2021.

[3] A.F. Al-Bakri, R. Martinek, M. Pelc, J. Zygarlicki, and A. Kawala-Sterniuk, "Implementation of a morphological filter for removing spikes from the epileptic brain signals to improve identification ripples," *Sensors*, vol. 22, no. 19, p. 7522, 2022.

[4] R. Martinek *et al.*, "Advanced bioelectrical signal processing methods: Past, present and future approach—part II: Brain signals," *Sensors*, vol. 21, no. 19, p. 6343, 2021.

[5] Y. Liu, Z. Liu, Y. Zhou, and Y. Tian, "Implantable electrochemical sensors for brain research," *JACS Au*, vol. 3, no. 6, pp. 1572–1582, 2023.

[6] R. Li, D. Yang, F. Fang, K.-S. Hong, A.L. Reiss, and Y. Zhang, "Concurrent fNIRS and EEG for brain function investigation: a systematic, methodology-focused review," *Sensors*, vol. 22, no. 15, p. 5865, 2022.

[7] W.-C. Su *et al.*, "Simultaneous multimodal fNIRS–EEG recordings reveal new insights in neural activity during motor execution, observation, and imagery," *Sci. Rep.*, vol. 13, no. 1, pp. 1–10, 2023.

[8] R. Li, C. Zhao, C. Wang, J. Wang, and Y. Zhang, "Enhancing fNIRS analysis using EEG rhythmic signatures: an eeg-informed fnirs analysis study," *IEEE Trans. Biomed. Eng.*, vol. 67, no. 10, pp. 2789–2797, 2020.

[9] R. Li, S. Li, J. Roh, C. Wang, and Y. Zhang, "Multimodal neuroimaging using concurrent EEG/fNIRS for poststroke recovery assessment: an exploratory study," *Neurorehabil. Neural Repair*, vol. 34, no. 12, pp. 1099–1110, 2020.

[10] L. Tong, "Evaluation of different brain imaging technologies," in *2021 International Conference on Public Art and Human Development (ICPAHD 2021)*. Atlantis Press, 2022, pp. 692–696.

[11] Z. Chen, C. Gao, T. Li, X. Ji, S. Liu, and M. Xiao, "Open access dataset integrating EEG and fNIRS during stroop tasks," *Sci. Data*, vol. 10, no. 1, p. 618, 2023.

[12] W. Bauer *et al.*, "Initial study on quantitative electroencephalographic analysis of bioelectrical activity of the brain of children with fetal alcohol spectrum disorders (FASD) without epilepsy," *Sci. Rep.*, vol. 13, no. 1, p. 109, 2023.

[13] M.N.A. Tawhid, S. Siuly, K. Wang, and H. Wang, "Automatic and efficient framework for identifying multiple neurological disorders from EEG signals," *IEEE Trans. Technol. Soc.*, vol. 4, no. 1, pp. 76–86, 2023.

[14] A. Kawala-Sterniuk *et al.*, "Influence of the variables describing brain signals on the performance of the Naive Bayesian Classifier," in *2022 Progress in Applied Electrical Engineering (PAEE)*. IEEE, 2022, pp. 1–5.

[15] A. Kawala-Sterniuk *et al.*, "Improving fNIRS signal quality using smoothing filtering," in *2023 Progress in Applied Electrical Engineering (PAEE)*. IEEE, 2023, pp. 1–8.

[16] S. Haufe *et al.*, "Elucidating relations between fMRI, ECoG, and EEG through a common natural stimulus," *NeuroImage*, vol. 179, pp. 79–91, 2018.

[17] H.Y. Kim, K. Seo, H.J. Jeon, U. Lee, and H. Lee, "Application of functional near-infrared spectroscopy to the study of brain function in humans and animal models," *Mol. Cells*, vol. 40, no. 8, p. 523, 2017.

[18] A. Ortega-Martinez *et al.*, "How much do time-domain functional near-infrared spectroscopy (fNIRS) moments improve estimation of brain activity over traditional fNIRS?" *Neurophotonics*, vol. 10, no. 1, p. 013504, 2023.

[19] K. Ji, D.Y. Chen, K.D. Karunakaran, and B.B. Biswal, "Altered brain hemodynamic response and cognitive function after sleep deprivation: a functional near-infrared spectroscopy study," *Brain-Apparatus Commun.-J. Bacomics*, vol. 2, no. 1, p. 2169589, 2023.

[20] A. Shah and A.-K. Seghouane, "An integrated framework for joint HRF and drift estimation and HbO/HbR signal improvement in fNIRS data," *IEEE Trans. Med. Imaging*, vol. 33, no. 11, pp. 2086–2097, 2014.

[21] H. Niu *et al.*, "Test-retest reliability of graph metrics in functional brain networks: a resting-state fNIRS study," *PLoS One*, vol. 8, no. 9, p. e72425, 2013.

[22] G. Lee, S.H. Jin, S.T. Yang, J. An, and B. Abibulaev, "Cross-correlation between HbO and HbR as an effective feature of motion artifact in fNIRS signal," in *2018 6th International Conference on Brain-Computer Interface (BCI)*. IEEE, 2018, pp. 1–3.

[23] J. Pereira, B. Direito, M. Lührs, M. Castelo-Branco, and T. Sousa, "Multimodal assessment of the spatial correspondence between fNIRS and fMRI hemodynamic responses in motor tasks," *Sci. Rep.*, vol. 13, no. 1, p. 2244, 2023.

[24] D.A. Boas and M.A. Franceschini, "Haemoglobin oxygen saturation as a biomarker: the problem and a solution," *Philos. Trans. R. Soc. A-Math. Phys. Eng. Sci.*, vol. 369, no. 1955, pp. 4407–4424, 2011.

[25] H.E. Shatzer and F.A. Russo, "Brightening the study of listening effort with functional near-infrared spectroscopy: A scoping review," in *Seminars in Hearing*. Thieme Medical Publishers, Inc., 2023.

[26] Z. Su *et al.*, "Time–frequency cross-coupling between cortical low-frequency neuronal calcium oscillations and blood oxygen metabolism evoked by ultrasound stimulation," *Cereb. Cortex*, vol. 33, no. 8, pp. 4665–4676, 2023.

[27] S.C. Bunce, M. Izzetoglu, K. Izzetoglu, B. Onaral, and K. Pourrezaei, "Functional near-infrared spectroscopy," *IEEE Eng. Med. Biol. Mag.*, vol. 25, no. 4, pp. 54–62, 2006.

[28] M. Pelc *et al.*, "Machine Learning-based cascade filtering system for fNIRS data analysis," in *2023 Progress in Applied Electrical Engineering (PAEE)*. IEEE, 2023, pp. 1–5.

[29] A. Kawala-Sterniuk *et al.*, "Comparison of smoothing filters in analysis of EEG data for the medical diagnostics purposes," *Sensors*, vol. 20, no. 3, p. 807, 2020.

[30] N.D. Schiff *et al.*, "Brain–computer interfaces for communication in patients with disorders of consciousness: A gap analysis and scientific roadmap," *Neurocrit. Care*, pp. 1–17, 2024.

[31] W. Qiu, X. Wang, D. Ma, J. Qiu, and W. Lu, "A recurrent neural network for adaptive filtering in terahertz time-domain spectroscopy," *Infrared Phys. Technol.*, vol. 138, p. 105256, 2024, doi: 10.1016/j.infrared.2024.105256.

[32] R. Janapati, V. Dalal, and R. Sengupta, "Advances in modern EEG–BCI signal processing: A review," *Mater. Today-Proc.*, vol. 80, pp. 2563–2566, 2023.

[33] D. Zapała, P. Augustynowicz, and M. Tokovarov, "Recognition of attentional states in VR environment: An fNIRS study," *Sensors*, vol. 22, no. 9, p. 3133, 2022.

[34] A. Kawala-Sterniuk *et al.*, "NERD = Neuroimaging EEG and fNIRS Dataset," Apr 2024, doi: 10.17605/OSF.IO/D5YRF. [Online]. Available: osf.io/d5yrf

[35] B. Kurdi, S. Lozano, and M.R. Banaji, "Introducing the open affective standardized image set (OASIS)," *Behav. Res. Methods*, vol. 49, pp. 457–470, 2017.

[36] B. Kurdi, S. Lozano, and M.R. Banaji, "Introducing the Open Affective Standardized Image Set (OASIS)," Oct 2021, doi: 10.17605/OSF.IO/6PND7. [Online]. Available: osf.io/6pnd7

[37] N. Browarska *et al.*, "Comparison of smoothing filters' influence on quality of data recorded with the Emotiv EPOC Flex brain-computer interface headset during audio stimulation," *Brain Sci.*, vol. 11, no. 1, p. 98, 2021.

[38] P.A. Valdes-Sosa *et al.*, "Model driven EEG/fMRI fusion of brain oscillations," *Human Brain Mapping*, vol. 30, no. 9, pp. 2701–2721, 2009.

[39] J.S. Barlow, "Methods of analysis of nonstationary EEGs, with emphasis on segmentation techniques: a comparative review," *J. Clinic. Neurophysiol.*, no. 3, pp. 267–304, 1985.

[40] J. Luo, K. Ying, and L. Bai, "Savitzky–Golay smoothing and differentiation filter for even number data," *Signal Process.*, vol. 85, pp. 1429–1434, 2005, doi: 10.1016/j.sigpro.2005.02.002.

[41] R.E. Kalman, "A new approach to linear filtering and prediction problems," *Trans. ASME–J. Basic Eng.*, vol. 82, no. Series D, pp. 35–45, 1960.

[42] A. Shtayat, S. Moridpour, B. Best, and H. Daoud, "Application of noise-cancelling and smoothing techniques in road pavement vibration monitoring data," *Int. J. Transp. Sci. Technol.*, vol. 14, pp. 110–119, 2024, doi: 10.1016/j.ijtst.2023.04.002.

[43] N. Raheja and A.K. Manocha, "Removal of artifcats in electrocardiograms using Savitzky-Golay Filter: An improved approach," *J. Inf. Technol. Manag.*, vol. 12, no. Special Issue: Deep Learning for Visual Information Analytics and Management., pp. 62–75, 2020.

[44] T. Pander, "EEG signal improvement with cascaded filter based on OWA operator," *Signal Image Video Process.*, vol. 13, no. 6, pp. 1165–1171, 2019.

[45] R. Alhalaseh and S. Alasasfeh, "Machine-learning-based emotion recognition system using EEG signals," *Computers*, vol. 9, no. 4, p. 95, 2020.

[46] F. Klein and C. Kranczioch, "Signal processing in fNIRS: a case for the removal of systemic activity for single trial data," *Front. Hum. Neurosci.*, vol. 13, p. 331, 2019, doi: 10.3389/fnhum.2019.00331.

[47] Y. Cimtay and E. Ekmekcioglu, "Investigating the use of pretrained convolutional neural network on cross-subject and cross-dataset EEG emotion recognition," *Sensors*, vol. 20, no. 7, p. 2034, 2020.

[48] P.W. Dans, S.D. Foglia, and A.J. Nelson, "Data processing in functional near-infrared spectroscopy (fNIRS) motor control research," *Brain Sci.*, vol. 11, no. 5, p. 606, 2021.

[49] G. Galanis and M. Anadranistakis, "A one-dimensional Kalman filter for the correction of near surface temperature forecasts," *Meteorolog. Appl.*, vol. 9, pp. 437–441, 2002.

[50] J. L. Guiñón, E. Ortega, J. García-Antón, and V. Pérez-Herranz, "Moving Average and Savitzki-Golay smoothing filters using mathcad," *Papers ICEE*, vol. 2007, pp. 1–4, 2007.

[51] R. Yadav, S. Tripathi, P. Gogumalla, and S. Dubey, "Trend analysis by Mann-Kendall test for precipitation and temperature for thirteen districts of uttarakhand," *J. Basic Eng.*, vol. 16, p. 164, 2014, doi: 10.54386/jam.v16i2.1507.

[52] C.P. Suárez-Araujo, Y. Cabrera-León, P. Fernández-López, and P.G. Báez, "Current trends on the early diagnosis of alzheimer's disease by means of neural computation methods," *Int. J. Electron. Telecommun.*, vol. 70, no. 2, pp. 277–283, 2024, doi: 10.24425/ijet.2024.149542.